

Non-isothermal crystallization kinetics of TiO₂ nanoparticle-filled poly(ethylene terephthalate) with structural and chemical properties

Harshita Agrawal · Kamendra Awasthi ·
Vibhav K. Saraswat

Received: 12 January 2014 / Revised: 3 March 2014 / Accepted: 23 March 2014
© Springer-Verlag Berlin Heidelberg 2014

Abstract The present research work includes non-isothermal crystallization kinetics of poly(ethylene terephthalate) (PET)–titanium dioxide (TiO₂) nanocomposites as well as structural and chemical properties of these nanocomposites. The average grain size of chemically synthesized TiO₂ nanoparticles has been calculated 19.31 nm by TEM and XRD. The morphology and structural analysis of PET–TiO₂ nanocomposites, prepared via solution casting method, has been investigated using SEM and XRD, respectively. The nature of chemical bonds has been discussed on the basis of FTIR spectra. The effect of TiO₂ nanoparticles and cooling rates on non-isothermal crystallization kinetics of PET was examined by differential scanning calorimetry at various heating and cooling rates. It has been observed that TiO₂ nanoparticles accelerate the heterogeneous nucleation in PET matrix. The crystallization kinetics could be explained through Avrami–Ozawa combined theory. TiO₂ nanoparticles cause to make molecular chains of PET easier to crystallize and accelerate the crystallization rates during non-isothermal crystallization process; this conclusion has also been verified by Kissinger model for crystallization activation energy.

Introduction

Recently, small amount of inorganic filler into polymers has been extensively utilized in an attempt to enhance the thermo-physical (e.g., structural, thermal properties, electrical and mechanical) properties [1–4], due to their unique

H. Agrawal · V. K. Saraswat (✉)
Department of Physics, Banasthali University, Tonk 304022, Rajasthan, India
e-mail: vibhav.spsl@gmail.com

K. Awasthi
Department of Physics, Malaviya National Institute of Technology, Jaipur 302017, Rajasthan, India

properties and possibility for numerous applications in modern technology [5–10], such polymer nanocomposites have been proved themselves as potential candidate among researchers. Poly(ethylene terephthalate) (PET) is a commodity polymer competing directly with polyethylene, polypropylene and polystyrene in the markets of food and beverage packaging. Being semicrystalline thermoplastic polyester [11], the thermal properties of PET are used in food packaging, peelable seals, lids, vacuum insulation panels, etc. In the packaging industry, to improve barrier performance to ultraviolet rays, as well as adding strength, stiffness, dimensional stability and heat resistance, polymer nanocomposites have been recognized as the next great frontier of materials [12]. PET is a slowly crystallizing polymer that can be obtained with different degrees of crystallinity (0–50 %) as a result of specific thermal and/or mechanical treatment to which it is submitted [13, 14].

Titanium dioxide (TiO_2) is commonly used inorganic filler for organic polymer matrix. It is wide band gap ($E_g = 3.2$ eV) semiconductor material [15]. The use of TiO_2 is advantageous over capping agents in the chemical reduction process of metal ions, as it is free from the blocking of active sites by organic capping agents [16]. Also, the inclusion of TiO_2 nanoparticles in polymer matrix results in the heterogeneous nucleation effect, which provides more sites for nucleation.

The literature review reveals that there has been much research on inorganic composites by adding nanoparticles to the polymer matrix. A plenty of work has been done to enhance the structural properties of PET. The FTIR spectrum of PET membranes, irradiated by O^{6+} ions, show minor changes in structural properties due to breakage of one or two bonds in the ladder structure, but it will not change the overall structure of polymer [17]. Jeziorny and Mo's methods have been applied to describe the kinetics of the non-isothermal crystallization process of PET matrix with incorporated surface-treated TiO_2 particles as well as pure nano- TiO_2 particles [18]. The crystallization behavior of PET-based nanocomposites containing 3 wt% of different nanoparticles (MontMorilloniTe—MMT; titanium dioxide— TiO_2 ; and silica dioxide— SiO_2) using DSC shows all fillers behave as nucleating agents for PET except SiO_2 that acts as inhibitor in case of direct injection molding (DIM) procedure [13]. The isothermal and non-isothermal crystallization kinetics of PET with three nucleating agents concluding talc, sodium benzoate (SB) and an ionomer (Ion. , Na^+) has been described using Avrami and Ozawa equations, respectively [19]. Non-isothermal crystallization kinetics of silica nanoparticle-filled poly(ethylene 2,6-naphthalate) (PEN) nanocomposites have been analyzed using Ozawa and Avrami theories and a combined method. Also, the crystallization activation energy has been calculated using Kissinger method [20]. The crystallization kinetics and the crystallization parameters of the alumina-filled PEEK nanocomposites have been described by Avrami, Ozawa and combined Avrami–Ozawa equations [21].

In this paper, the effect of TiO_2 nanoparticle inclusion in PET matrix with structural and thermal properties has been reported. Although, there are similar studies that have been carried out on PET with different fillers, PET– TiO_2 nanocomposites are not widely reported. We concentrate on structural changes and non-isothermal crystallization kinetics in PET– TiO_2 nanocomposites, which are characterized by XRD, FTIR and DSC techniques.

Experimental

Materials and sample preparation

TiO₂ nanoparticles have been synthesized by chemical method [15]. TiCl₃ solution has been mixed with NH₄OH (100 mM) aqueous solution in 1:6 volume ratio; PH of solution has increased up to 2.0. The resulting solution has been stirred for 48 h at room temperature. The precipitate, obtained by centrifuging, has been further washed in iso-propyl alcohol and dried at room temperature.

PET–TiO₂ nanocomposites have been prepared by solution casting method. PET (Sigma-Aldrich, USA) was dissolved in DCM (Sigma-Aldrich, Germany, $d = 1.325 \text{ g mmol}^{-1}$) with 2 % Trifluoroacetic acid (TFA) (Merck, India). TiO₂ nanoparticles have been added in this PET solution according to wt%. After stirring for 2 h, the solution has been casted on mercury bath. In this manner, the PET–TiO₂ nanocomposites (1, 2 and 3 wt% of TiO₂ nanoparticle) have been prepared.

X-Ray diffraction

The size of TiO₂ nanoparticles has been subjected to X-rays, and diffractogram has been recorded using X-ray diffractometer Bruker D8 Advance with CuK _{α} radiation in the range of 20°–70° ($\lambda = 0.1506 \text{ nm}$). To confirm the crystallite size, the structural analysis of PET–TiO₂ nanocomposites has also been carried out by the same XRD machine.

Fourier transform infrared (FTIR)

The changes in chemical bonds and modifications have been analyzed by Fourier transform infrared (FTIR) spectroscopy. FTIR spectroscopy has been performed in transmission mode using Agilent (CARY 660) FTIR spectrometer in the range 500–3,500 cm^{−1}.

Differential scanning calorimetry (DSC)

Non-isothermal crystallization kinetics of TiO₂ nanoparticle-filled PET composites has been studied using NETZSCH DSC 204 F1 Phoenix and the weight of all samples has been taken 6–7 mg approximately. The samples have been subjected to heat treatment up to 300 °C with different heating rates (5, 10, 15 and 20 °C min^{−1}) under nitrogen atmosphere of 40–50 ml min^{−1}, and held for 5 min to remove its previous thermal history. The crystallization kinetics investigated by cooling these samples from 300 to 30 °C with the same cooling rate corresponds to that particular heating rate.

Results and discussion

Figure 1a shows the TEM micrograph of TiO₂ nanoparticles and Fig. 1b shows the XRD pattern of TiO₂ nanoparticles. The average particle size of TiO₂ nanoparticles

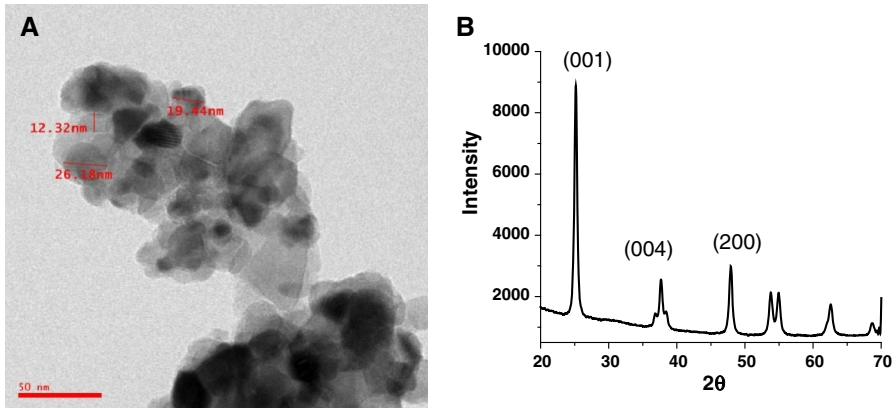


Fig. 1 **a** TEM image of TiO₂ nanoparticles with size determination, **b** XRD pattern of TiO₂ nanoparticles

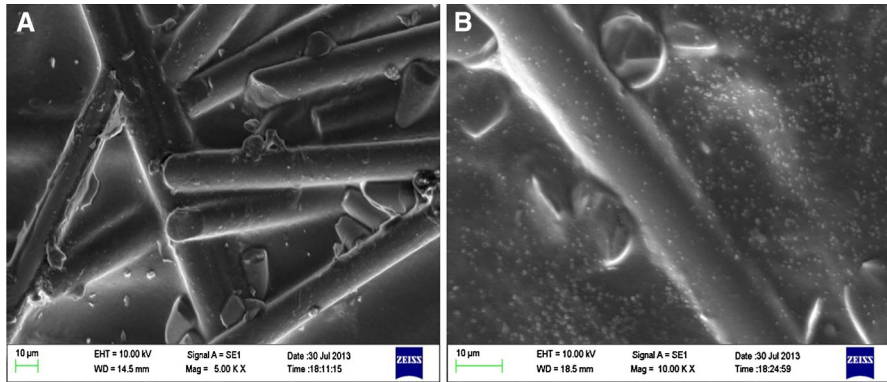


Fig. 2 SEM micrographs of PET–TiO₂ nanocomposites; **a** PET Pristine and **b** PET + 2 % TiO₂

has been calculated by TEM image (Fig. 1a) that found to be 19.31 nm. Clear and homogeneous spherical structure of TiO₂ nanoparticles can be seen in TEM image. And also, it has been confirmed through XRD pattern (Fig. 1b) using Debye–Scherrer’s formula [22].

PET nanocomposite morphology with different concentration of TiO₂ nanoparticles can be seen in Fig. 2. It can be explained from SEM micrographs (Fig. 2) that TiO₂ nanoparticles have been homogeneously dispersed in PET matrix. A long cylindrical fiber-like structure is representing the PET matrix, and the small spherical nanoparticles are embedded among these polymer fibers.

Structural properties

The XRD patterns of pristine PET and PET/TiO₂ composites have been shown in Fig. 3. As it is clear from XRD of TiO₂ nanoparticles (Fig. 1) that the major

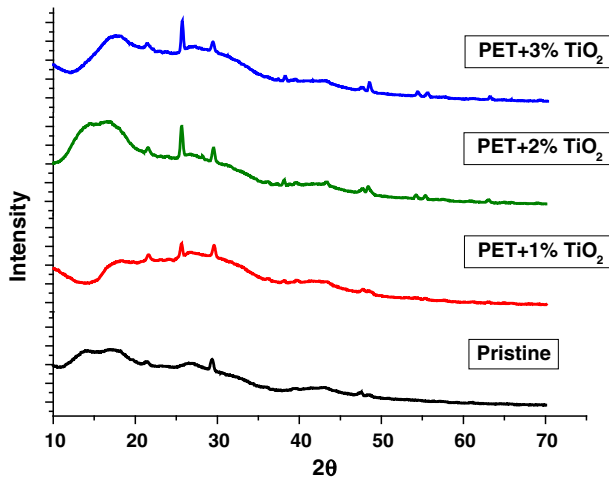


Fig. 3 XRD patterns of PET–TiO₂ nanocomposites

peak (001) comes at 25° which can be seen in composite XRD also. In the pristine XRD pattern, there is a single small peak because PET is semicrystalline material. With the incorporation of TiO₂ nanoparticles, the peak (001) appears clearly with increasing wt% of nanoparticles. This is the reflection of small changes in structure of semicrystalline PET by inclusion of TiO₂ nanoparticles.

Chemical properties

FTIR spectra of PET pristine and PET–TiO₂ nanocomposites are shown in Fig. 4. The type and nature of chemical bonds have been analyzed by these IR spectra. It is well-known fact that in a polymer each molecular group has characteristic frequencies of vibrational and rotational oscillations that lie in infrared (IR) and microwave region, respectively [17].

In spectra of pristine PET, peak observed at 1,723 cm^{−1} corresponds to the strong C=O stretching bond of aromatic carboxylic acid. Whereas, the peaks at 2,968 and 2,229 cm^{−1} correspond to C–H stretching of ethylene group. IR peaks in the range 1,000–1,200 cm^{−1} show C–O stretching. The transmittance of three bands has been analyzed: 3,450 cm^{−1} due to OH[−] stretching, 1,404 cm^{−1} due to CH₂ bending and 721 cm^{−1} due to C–H bending of di-substitute benzene.

After the inclusion of TiO₂ nanoparticles in PET matrix, the peaks have been found corresponding to Ti–O bond also. The appeared peaks at 547, 551, 593 cm^{−1} in PET/TiO₂ nanocomposites for 1, 2 and 3 wt% TiO₂, respectively, indicate Ti–O vibrations. The intensity of peak corresponding to 586 cm^{−1} decreases with increasing TiO₂ filler which results in the decreasing polarity.

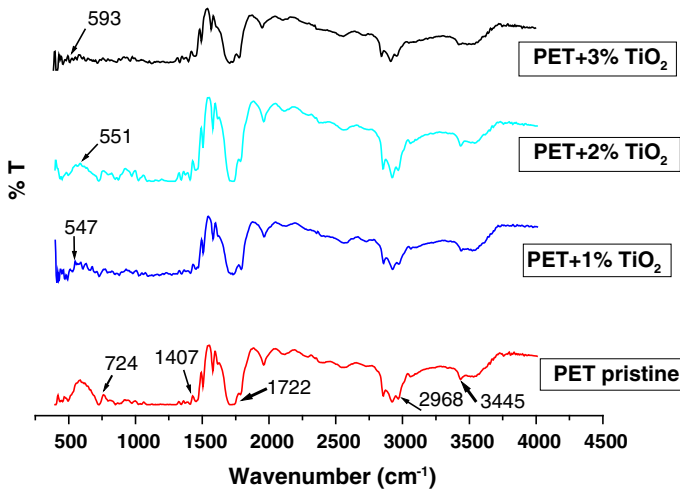


Fig. 4 FTIR spectra of pristine and PET–TiO₂ nanocomposites

Crystallization behavior

The crystallization peaks during cooling of PET–TiO₂ nanocomposites at different cooling rates are shown in Fig. 5. It is clearly observed that for all samples, a cooling rate is increased, the crystallization onset temperature (T_s), peak temperature (T_p) and end temperature (T_e), shift to lower temperature side. The crystallization is a two-step phenomena: nucleation and growth. When PET and its nanocomposites have been subjected to cooling from a temperature above, its melting temperature, due to heterogeneous nucleation, growth of new phase particles plays a major role in lowering the crystallization temperature.

The effect of cooling rates and filler content on the overall crystallization time, t_c , can be determined as follows [20]:

$$t_c = \frac{T_s - T_e}{a}, \quad (1)$$

where a is the cooling rate, T_s is the initial crystallization temperature, and T_e is final crystallization temperature. It is evident from Fig. 6 that inclusion of TiO₂ nanoparticle in PET matrix may cause to reduce the overall crystallization time. Also, the lower T_c is observed for higher cooling rates (Fig. 5). These results could be explained through the heterogeneous nucleation effect. The shorter crystallization time accelerates the rapid heterogeneous nucleation and smaller crystal grain size which may cause lower crystal growth [21]. The values of crystallization parameters, derived from Fig. 5 have been listed in Table 1.

The absolute crystallinity fraction X_c at different cooling rates has been calculated using following relation [20]:

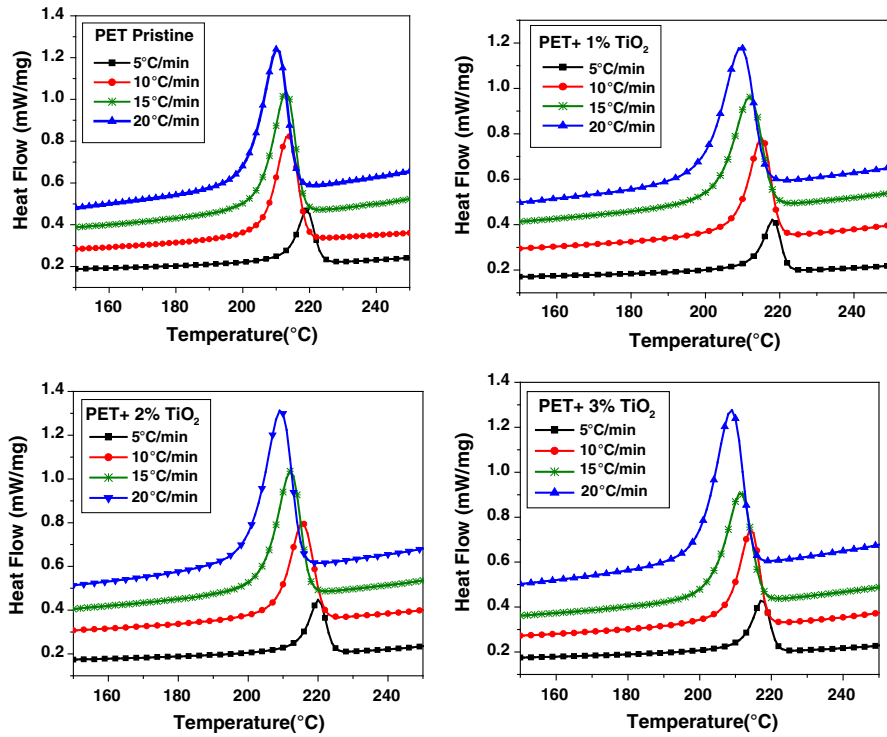


Fig. 5 DSC thermograms of pristine and PET–TiO₂ nanocomposites

$$X_c = \frac{\Delta H_c}{\Delta H_f^0 W_{\text{polymer}}} \times 100, \quad (2)$$

where $\Delta H_f^0 \sim 140 \text{ J g}^{-1}$ and W_{polymer} is the weight fraction of the polymer matrix. As listed in Table 1, the degree of crystallinity has been increased by addition of TiO₂ filler content. This may be accounted for TiO₂ nanoparticles acting as nucleation agent in PET matrix under non-isothermal crystallization condition [20]. Since, degree of crystallinity affects the extent of the intermolecular secondary bonding, it can have a rather significant influence on the mechanical properties of PET. Increasing the crystallinity of polymer generally enhances its strength [23]. As described before that PET is commonly used in packaging and bottles, the nanocomposites with TiO₂ nanoparticles will be better used in these applications.

Non-isothermal crystallization kinetics

The relative crystallinity $X_c(T)$ at different cooling rates for DSC thermograms can be determined by the following equation [20]:

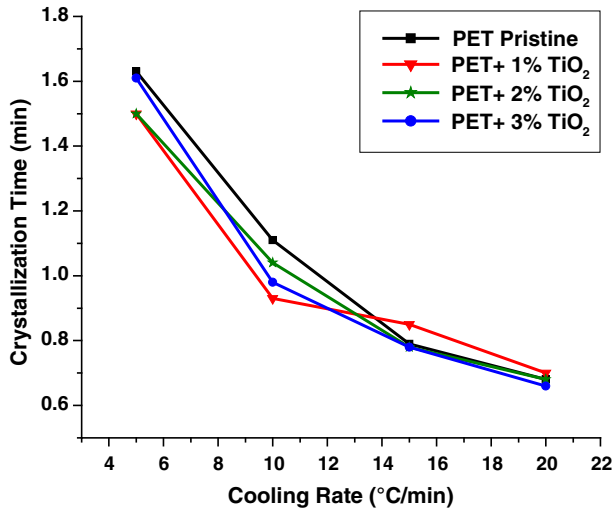


Fig. 6 Overall crystallization time for PET–TiO₂ nanocomposites at various cooling rates

$$X_c(T) = \frac{\int_{T_0}^T \left(\frac{dH_c}{dT}\right) dT}{\int_{T_0}^{T_\infty} \left(\frac{dH_c}{dT}\right) dT}, \quad (3)$$

where T_0 and T_∞ are the temperatures at which the crystallization starts and ends; A_0 and A_∞ are areas under the normalized DSC curves. The relative crystallinity as a function of temperature has been shown in Fig. 7. The similar sigmoidal shapes can be seen in all the curves. Also, the spherulite impingement in the later stage of crystallization may result in the curvature of the upper part of the plots.

For the non-isothermal process, the relation between crystallization time and temperature has been shown in Fig. 8, using Eq. 4, that is:

$$t = \frac{|T_0 - T|}{a} \quad (4)$$

It is clearly evident from Fig. 8 that the inclusion of nanoparticles results less crystallization time to reach the same relative crystallinity in comparison to pristine PET.

Ozawa model

The crystallization mechanism of polymers can be explained through Ozawa theory which assumes that the crystallization occurs at constant cooling rate a [24], gives relative degree of crystallinity, $X_c(T)$ at temperature T , as follows;

$$1 - X_c(T) = \exp \left[-\frac{K(T)}{|a|^m} \right] \quad (5)$$

$$\log[-\ln(1 - X_c(T))] = \log K(T) - m \log a, \quad (6)$$

Table 1 Crystallization parameters of PET–TiO₂ nanocomposites

Sample	Cooling rate (°C min ⁻¹)	<i>T</i> _m (°C)	<i>T</i> _s (°C)	<i>T</i> _p (°C)	<i>T</i> _c (°C)	<i>H</i> _c (J g ⁻¹)	<i>X</i> _c (%)
Pristine PET	5	253.7	214.54	219.25	222.71	15.96	11.4
	10	253.43	207.78	213.53	217.79	18.14	12.9
	15	253.8	205.77	213.11	217.65	18.43	13.2
	20	252.62	202.03	210.24	215.71	18.85	13.3
PET + 1 % TiO ₂	5	246.86	214.00	218.22	221.51	13.75	9.72
	10	253.7	209.73	215.13	219.11	15.8	11.1
	15	253.92	204.49	211.95	217.23	16.12	11.4
	20	252.98	201.08	209.45	215.24	17.25	12.1
PET + 2 % TiO ₂	5	253.37	215.74	220.11	223.53	14.95	10.5
	10	253.78	210.02	215.53	220.45	16.63	11.7
	15	253.23	205.11	212.03	216.90	17.78	12.4
	20	253.81	200.92	209.29	214.58	19.74	13.8
PET + 3 % TiO ₂	5	245.1	212.85	217.36	220.90	14.5	10.0
	10	252.93	208.58	214.23	218.40	14.88	10.3
	15	254.68	204.54	211.39	216.37	15.5	10.7
	20	254.36	200.81	208.83	214.16	18.36	12.7

where $K(T)$ is a cooling function depending on the overall crystallization rate at temperature T , m is the Ozawa exponent depending on the dimension of crystal growth and a is the cooling rate. Figure 9 illustrates the plot between $\log [-\ln (1 - X_c(T))]$ and $\log a$ according to the Ozawa theory. $K(T)$ and m could be determined by slope and the intercept, respectively.

The deviation from linearity of curves suggests that these samples do not follow Ozawa model consumptions. The Ozawa model is based on the quasi-isothermal crystallization; under the non-isothermal crystallization, the function of both time and cooling rate can be constant for much duration but not the crystallization rate. Also, there should be explanation of slow secondary crystallization and folded chain length of polymer chains. Folded chain length is a function of the crystallization temperature. Under dynamic crystallization, the folded chain should be different; that is why, the folded chain length should be taken theoretically in the derivation of crystallization [25].

Avrami model

Another theory given by Avrami can be applied to analyze the non-isothermal crystallization of PET–TiO₂ nanocomposites. This model assumes that relative crystallinity at given time ($X_c(t)$) increases with crystallization time (t) [26, 27].

$$1 - X_c(t) = \exp(-Z_t t^n) \quad (7)$$

$$\log[-\ln(1 - X_c(t))] = n \log t + \log Z_t, \quad (8)$$

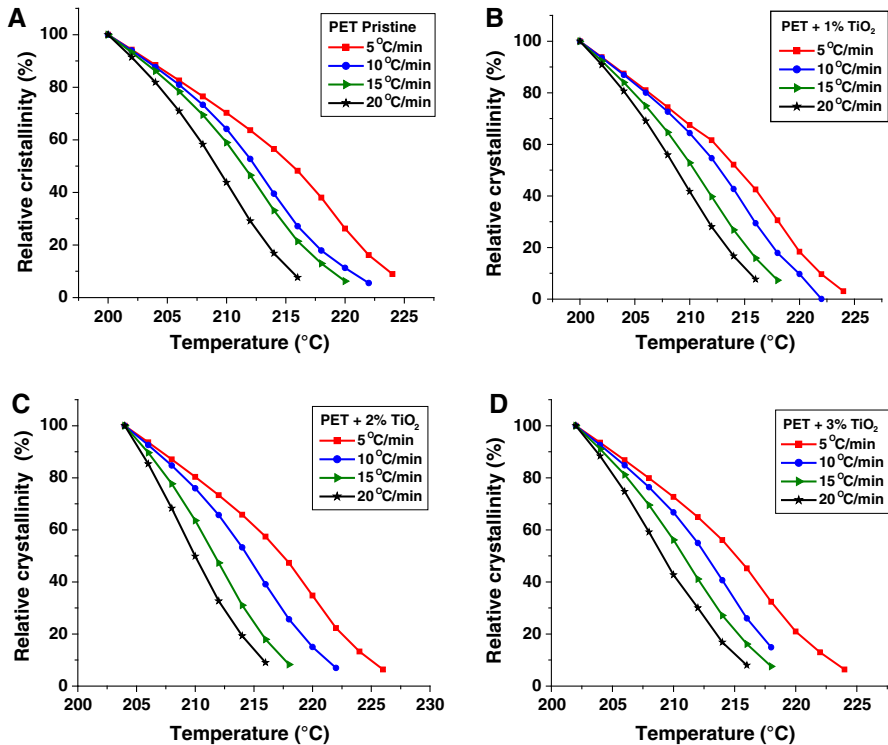


Fig. 7 Relative crystallinity (%) vs. temperature for non-isothermal crystallization at various cooling rates: **a** pristine PET, **b** PET + 1 % TiO₂, **c** PET + 2 % TiO₂, **d** PET + 3 % TiO₂

where $X_c(t)$ is the relative degree of crystallinity at time t , Z_t is a growth rate constant involving both nucleation and growth rate parameters, and the exponent n is a mechanism constant with a value depending on the type of nucleation and the growth dimension. In the non-isothermal process, cooling rate effects are involved, so, the value of Z_t calculated from Eq. 8 should be corrected as [28]:

$$\log Z_c = \frac{\log Z_t}{a}. \quad (9)$$

According to Eq. 8, Fig. 10 shows the plot between $\log [-\ln (1-X_c(t))]$ and $\log t$. The good linear trend has been observed in graph except later stage.

The Ozawa exponent ' m ' and Avrami exponent ' n ' are listed in Table 2, from Eqs. 6 and 8, respectively. And the growth parameter ' Z_c ' (summarized in Table 3) has been calculated from Eq. 9.

As the Ozawa exponent ' m ' represents growth morphology and Avrami exponent ' n ' represents the dimensional growth, both values are higher in PET-TiO₂ nanocomposites in comparison to pure PET, indicating that the TiO₂ nanoparticles acted as heterogeneous nuclei for the initial nucleation. Therefore, the type of nucleation and the geometry of crystal growth of PET were significantly changed by the presence of the TiO₂ nanoparticles. The Avrami exponent n of PET ranged from

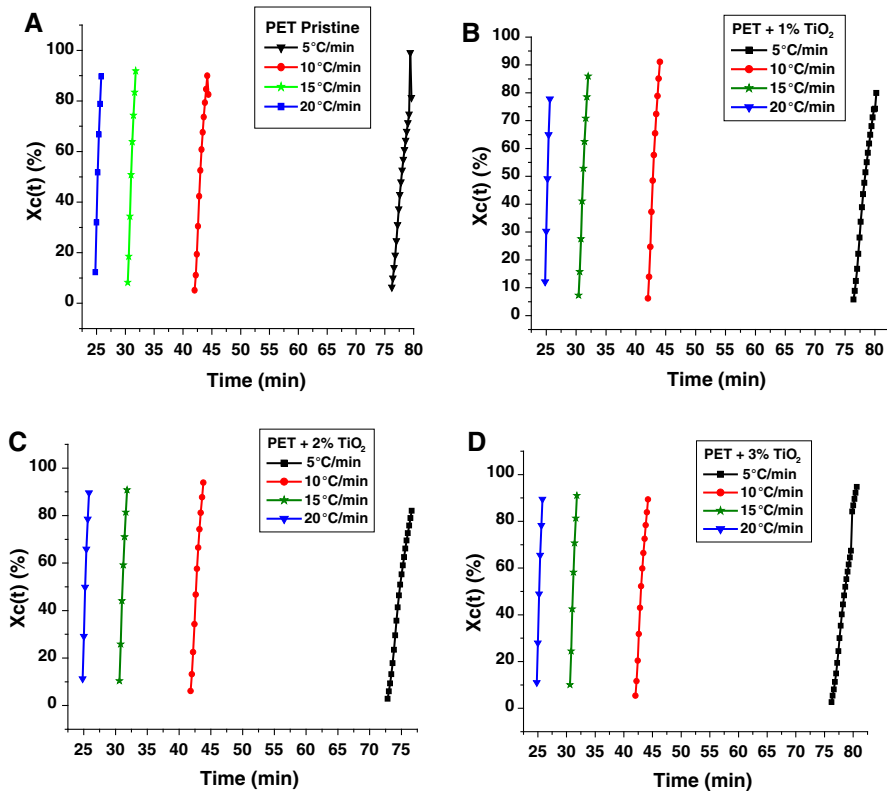


Fig. 8 Relative crystallinity vs. time for non-isothermal crystallization at various cooling rates: **a** pristine PET, **b** PET + 1 % TiO₂, **c** PET + 2 % TiO₂, **d** PET + 3 % TiO₂

1 to 2 which indicated that the rod-like growth occurred with homogeneous nucleation.

Combined Ozawa–Avrami model

It can be concluded that both Avrami and Ozawa models are not describing dynamic crystallization of PET and PET–TiO₂ nanocomposites. In these theories, the degree of crystallinity has been related to the cooling rate ‘*a*’ and the crystallization time *t* or temperature *T*. Liu et al. [29] proposed a combined model, which relates cooling rate ‘*a*’ to crystallization time ‘*t*’ for a particular degree of crystallinity. By combining Eqs. 6 and 8, a new kinetic equation for non-isothermal crystallization has been derived:

$$\log Z_t + n \log t = \log K(T) - m \log a \quad (10)$$

$$\log a = \log F(T) - b \log t, \quad (11)$$

where *b* is the ratio of Avrami and Ozawa exponent ($b = n/m$) and parameter $F(T) = [K(T)/Z_t]^{1/m}$, which indicates the required value of cooling rate approaching

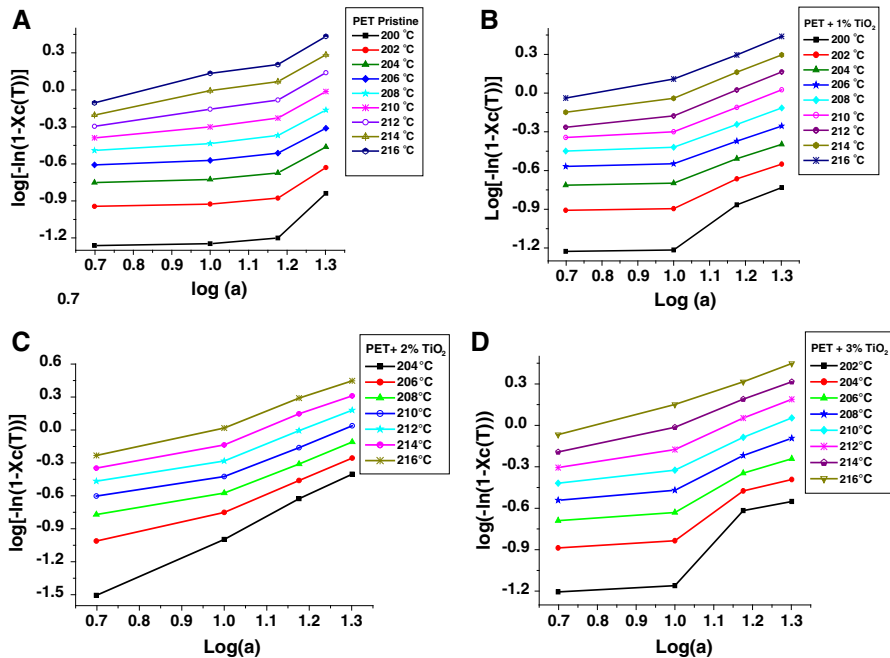


Fig. 9 Ozawa plots of $\log [-\ln (1-X_c(T))]$ vs. $\log a$ for non-isothermal crystallization: **a** pristine PET, **b** PET + 1 % TiO_2 , **c** PET + 2 % TiO_2 , **d** PET + 3 % TiO_2

to the degree of crystallinity at unit crystallization time [30]. In Fig. 11, a linear relationship is obtained by plotting curve between $\log a$ and $\log t$ at a particular degree of crystallinity according to Eq. 11. The values of $F(T)$ and ‘ $-b$ ’ have been determined by intercepts and slope of these plots, respectively.

The values of b and $\log F(T)$ are tabulated in Table 4; the $\log F(T)$ value increases with increase in degree of crystallinity value, which indicate the fact that high cooling rate is required for high degree of crystallinity. The linear relationship of plots is showing that the combined Avrami–Ozawa equations accurately defining the crystallization kinetics of PET– TiO_2 nanocomposites. This combined Avrami–Ozawa model has accurately been employed to describe the crystallization kinetics of alumina nanoparticle-filled poly (ether ether ketone) [21], surface-treated TiO_2 on poly (trimethylene terephthalate) (PTT) nanocomposites [31], Montmorillonite-filled polypropylene nanocomposites [32].

It could be concluded from Table 3 that the b values of TiO_2 -filled PET are higher than those of pristine PET. As described above, b equals to n/m where n is Avrami exponent; the n values of PET– TiO_2 nanocomposites are more than those of pure PET, and consequently, the reason can be clarified.

Crystallization activation energy

For evaluation of activation energy of non-isothermal crystallization kinetics at various cooling rates, the model proposed by Kissinger [33] is commonly used:

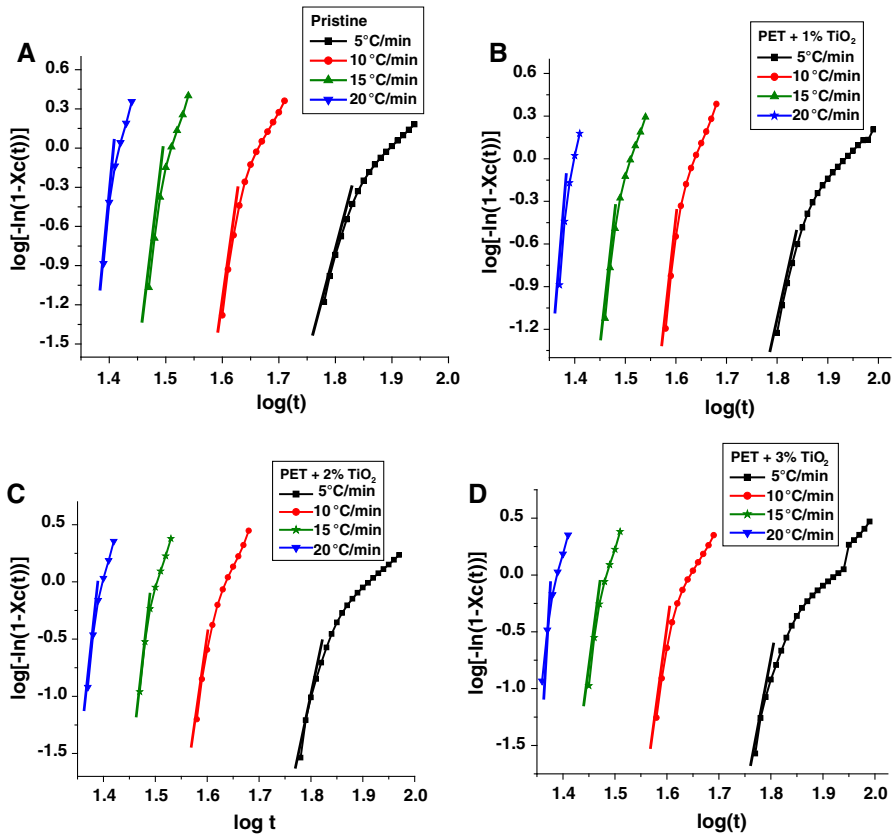


Fig. 10 Avrami plots of $\log [-\ln (1-X_c(t))]$ vs. $\log t$ for non-isothermal crystallization: **a** pristine PET, **b** PET + 1 % TiO_2 , **c** PET + 2 % TiO_2 , **d** PET + 3 % TiO_2

$$\frac{\left[\ln \left(\frac{a}{T_p^2} \right) \right]}{d \left(\frac{1}{T_p} \right)} = \frac{-\Delta E}{R}, \quad (12)$$

where R is the universal gas constant. Figure 12 shows the plot between $\ln(a/T_p^2)$ and $1/T_p$ for pure PET and PET- TiO_2 nanocomposites and, accordingly the crystallization activation energy could be determined by slope of the plots. Table 5 lists the activation energy of different samples for non-isothermal crystallization kinetics.

This is well-known fact that crystallization activation energy is the energy required to initiate non-isothermal crystallization. The above results verify that TiO_2 nanoparticles cause to make molecular chains of PET easier to crystallize and accelerate the crystallization rates during non-isothermal crystallization process, i.e., the TiO_2 nanoparticles are the favorable nucleating agents for heterogeneous nucleation.

Table 2 Values of Ozawa exponent ' m ' and Avrami exponent ' n '

Sample	Ozawa exponent ' m '	Avrami exponent ' n '
Pristine PET	0.624	1.624
PET + 1 % TiO ₂	0.727	1.727
PET + 2 % TiO ₂	1.344	2.344
PET + 3 % TiO ₂	0.932	1.932

Table 3 Avrami exponent n and the growth rate constant Z_c for non-isothermal crystallization of PET–TiO₂ nanocomposites

Sample	Cooling rate (°C min ⁻¹)	$Z_c \times 10^3$ (min °C ⁻¹)
Pristine PET	5	4.1
	10	15.4
	15	31.4
	20	79.1
PET + 1 % TiO ₂	5	3.0
	10	9.6
	15	42.9
	20	81.6
PET + 2 % TiO ₂	5	0.1
	10	12.0
	15	26.7
	20	70.8
PET + 3 % TiO ₂	5	0.1
	10	6.9
	15	29.1
	20	71.8

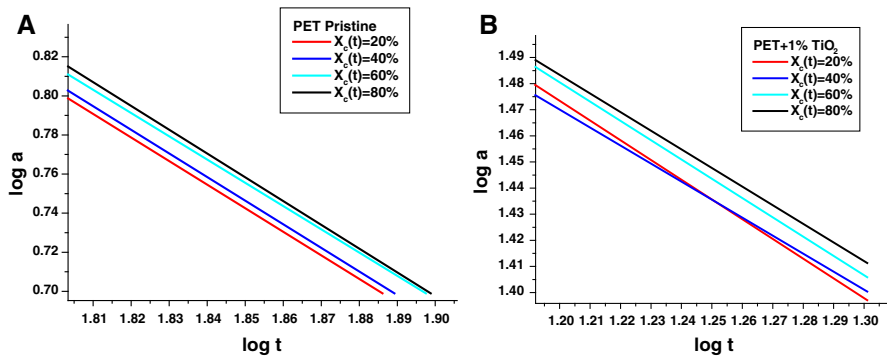
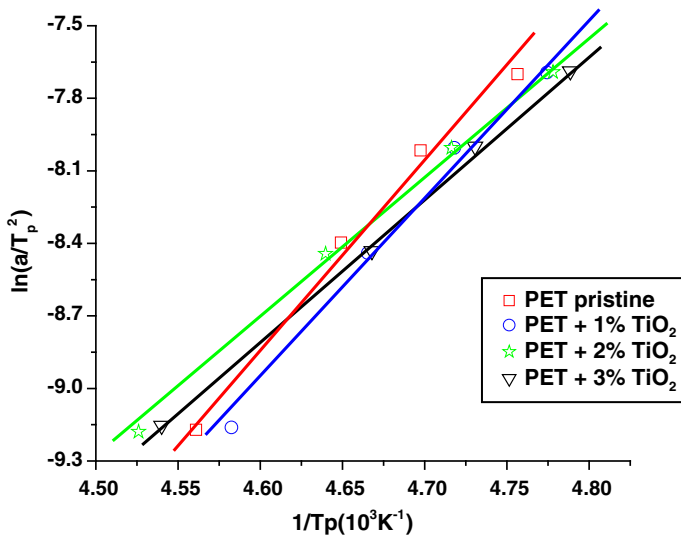
**Fig. 11** Combined Avrami–Ozawa plots of $\log a$ vs. $\log t$ for non-isothermal crystallization: **a** pristine PET, **b** PET + 1 % TiO₂

Table 4 The values of b and $F(T)$ versus degree of crystallinity for non-isothermal crystallization of PET–TiO₂ nanocomposites

Sample	Avrami–Ozawa parameter							
	$X_c(t)$ (20 %)		$X_c(t)$ (40 %)		$X_c(t)$ (60 %)		$X_c(t)$ (80 %)	
	b	$\log F(T)$	b	$\log F(T)$	b	$\log F(T)$	b	$\log F(T)$
PET pristine	1.218	2.991	1.216	2.994	1.209	2.988	1.212	3.019
PET + 1 % TiO ₂	1.222	3.001	1.217	2.991	1.22	3.006	1.225	3.02
PET + 2 % TiO ₂	1.276	3.08	1.273	3.079	1.264	3.069	1.26	3.021
PET + 3 % TiO ₂	1.218	2.99	1.216	2.992	1.205	2.982	1.28	3

Table 5 Values of activation energy for non-isothermal crystallization kinetics according to Kissinger model

Sample	Crystallization activation energy (kJ mol ⁻¹)
PET pristine	63.68
PET + 1 % TiO ₂	49.30
PET + 2 % TiO ₂	45.23
PET + 3 % TiO ₂	42.98

**Fig. 12** Crystallization activation energy plots for PET pristine and PET–TiO₂ nanocomposites

Conclusion

The SEM micrographs of TiO₂ nanoparticle-filled PET show the homogeneous dispersion of nanoparticles in PET matrix. As PET is a semicrystalline polymer, the

increased crystalline nature with inclusion of TiO_2 nanoparticles could be seen in XRD patterns. FTIR spectra show some changes in chemical bond structure in PET after inclusion of TiO_2 nanoparticles.

Under non-isothermal crystallization, the crystallization peak shifts to lower temperature with increasing cooling rate. And, with increasing content of TiO_2 nanoparticles, peak shifts to higher temperature. The overall crystallization time has also been reduced by TiO_2 content. The degree of crystallinity is increased by higher cooling rate. The Avrami and Ozawa theories have been proved to be inadequate individually, to explain the non-isothermal crystallization of PET– TiO_2 nanocomposites but the model given by Liu et.al (combined Avrami and Ozawa theories) has been successful employed to describe non-isothermal crystallization. The increasing parameter $\log F(T)$ with content of TiO_2 shows increased crystallization rate. When applied Kissinger model, reduced activation energy indicates that TiO_2 nanoparticles cause to make molecular chains of PET easier to crystallize and accelerate the crystallization rates during non-isothermal crystallization process.

Acknowledgments Authors are thankful to DST, Govt. of India. DST has granted sophisticated research facilities to Banasthali Vidyapith under its CURIE scheme. One of author (KA) is thankful to DST-New Delhi for funding under INSPIRE faculty award.

References

1. Saujanya C, Radhakrishnan S (2000) Structure development and crystallization behavior of PP/nanoparticulate composite. *Polymer* 42:6723–6731
2. Nelson JK, Fothergill JC (2004) Internal charge behavior of nanocomposites. *Nanotechnology* 15:586–595
3. Zhu J, Wilkie CA (2000) Thermal and fire studies on polystyrene-clay nanocomposites. *Polym Int* 49:1158–1163
4. Meneghetti P, Qutubuddin S (2006) Synthesis, thermal properties and application of polymer clay nanocomposites. *Thermochim Acta* 442:74–77
5. Beecroft LL, Ober CK (1997) Nanocomposite materials for optical applications. *Chem Mater* 9:1302–1317
6. Gangopadhyay R, De A (2000) Conducting polymer nanocomposites: a brief overview. *Chem Mater* 12:608–622
7. Ray SS, Bousmina M (2005) Biodegradable polymers and their layered silicate nanocomposites: in greening the 21st century materials world. *Prog Mater Sci* 50:962–1079
8. Tan EPS, Lim CT (2006) Mechanical characterization of nanofibers—a review. *Compos Sci Technol* 66:1102–1111
9. Sorrentino A, Gorrasi G, Vittoria V (2007) Potential perspectives of bio-nanocomposites for food packaging applications. *Trends Food Sci Tech* 18:84–95
10. Leszczyńska A, Njuguna J, Pielichowski K, Banerjee JR (2007) Polymer/montmorillonite nanocomposites with improved thermal properties: part I. Factors influencing thermal stability and mechanisms of thermal stability improvement. *Thermochim Acta* 453:75–96
11. Fried JR (2009) *Polymer science and technology*, 2nd edn. PHI, New Delhi
12. Todorov LV (2010) Multiscale morphology evolution of PET and its nanocomposites under deformation. Ph.D. thesis, Universidade do Minho Escola de Engenharia
13. Todorov LV, Viana JC (2007) Characterization of PET nanocomposites produced by different melt-based production methods. *J Appl Polym Sci* 106:1659–1669
14. Viana JC, Alves NM, Mano JF (2004) Morphology and mechanical properties of injection molded poly (ethylene terephthalate). *Polym Eng Sci* 44:2174–2184

15. Borse PH, Kankate LS, Dassenoy F, Vogel W, Urban J, Kulkarni SK (2002) Synthesis and investigations of rutile phase TiO_2 nanoparticles. *J Mater Sci Mater Electron* 13:553–559
16. Rodgers J, Delhom C, Hinchliffe D, Kim HJ, Cui X (2013) A rapid measurement for cotton breeders of maturity and fineness from developing and mature fibers. *Text Res J* 83(14):1439–1451
17. Awasthi K, Kulshrestha V, Avasthi DK, Vijay YK (2010) Optical, chemical and structural modification of oxygen irradiated PET. *Radiat Meas* 45:850–855
18. Zhu X, Wang B, Chen S, Wang C, Zhang Y, Wang H (2008) Synthesis and non-isothermal crystallization behavior of PET/surface-treated TiO_2 nanocomposites. *J Macromol Sci R Part B Phys* 47:1117–1129
19. Jiang XL, Luo SJ, Sun K, Chen XD (2007) Effect of nucleating agents on crystallization kinetics of PET. *Express Polym Lett* 1(4):245–251
20. Kim SH, Ahn SH, Hirai T (2003) Crystallization kinetics and nucleation activity of silica nanoparticle-filled poly (ethylene 2, 6-naphthalate). *Polymer* 44:5625–5634
21. Kuo MC, Huang JC, Chen M (2006) Non-isothermal crystallization kinetic behavior of alumina nanoparticle filled poly (ether ether ketone). *Mater Chem Phys* 99:258–268
22. Qiu S, Kalita S (2006) Synthesis, processing and characterization of nanocrystalline titanium dioxide. *J Mater Sci Eng A* 327:435–436
23. Callister WD, Rethwisch DG (2009) Materials science and engineering. John Wiley and Sons publication, USA
24. Ozawa T (1971) Kinetics of non-isothermal crystallization. *Polymer* 12(3):150–158
25. Di Lorenzo ML, Silvestre C (1999) Non-isothermal crystallization of polymers. *Prog Polym Sci* 24(6):917–950
26. Avrami M (1939) Kinetics of phase change, I. General theory. *J Chem Phys* 7:1103–1112
27. Avrami M (1941) Kinetics of phase change III. *J Chem Phys* 9:177–184
28. Lu XF, Hay JN (2001) Isothermal crystallization kinetics and melting behaviour of poly (ethylene terephthalate). *Polymer* 42(23):9423–9431
29. Liu T, Mo Z, Wang S, Zhang H (1997) Nonisothermal melt and cold crystallization kinetics of poly(aryl ether ether ketone ketone). *Polym Eng Sci* 37(3):568–575
30. Weng W, Chen G, Wu D (2003) Crystallization kinetics and melting behaviors of nylon 6/foiled graphite nanocomposites. *Polymer* 44:8119–8132
31. Ramesh V, Mohanty S, Panda BP, Nayak SK (2013) Nucleation effect of surface treated TiO_2 n poly (trimethylene terephthalate) (PTT) nanocomposites. *J Appl Polym Sci* 127(3):1909–1920
32. Xu W, Ge M, He P (2002) Nonisothermal crystallization kinetics of polypropylene/montmorillonite nanocomposites. *J Polym Sci Part B Polym Phys* 40:408–414
33. Kissinger HE (1956) Variation of peak temperature with heating rate in differential thermal analysis. *J Res Natl Bur Stand* 57:217–221